17th World Conference on Earthquake Engineering, 17WCEE
Sendai, Japan - September 13th to 18th 2020

SEISMIC REHABILITATION OF SUBSTANDARD INTERIOR RC BEAM-COLUMN JOINTS BY ECC-INFILLED STEEL CYLINDER SHELL

F. Lin[(1)], H. Qian[(2)], J. Guo[(3)], X. Yang[(4)]

[(1)] *Professor, Dr, Department of Structural Engineering, Tongji University, 1239 Siping Road, Shanghai 200092, PR China, lin_feng@tongji.edu.cn*
[(2)] *Graduate Student, Department of Structural Engineering, Tongji University, 1239 Siping Road, Shanghai 200092, PR China, 1910295@tongji.edu.cn*
[(3)] *Graduate student, Department of Structural Engineering, Tongji University, 1239 Siping Road, Shanghai 200092, PR China, 1530584@tongji.edu.cn*
[(4)] *Graduate student, Department of Structural Engineering, Tongji University, 1239 Siping Road, Shanghai 200092, PR China, yxmbyd@163.com*

Abstract

Reinforced concrete (RC) framed structures that were constructed prior to the 1970s, especially those in earthquake-prone areas, have significant deficiencies in the beam-column joint regions due to insufficient or no transverse reinforcement. As a result, the substandard beam-column joints in existing structures are likely to fail in a brittle manner prior to the formation of plastic hinges in the connected beams, which may lead to the entire collapse of buildings. Therefore, it is of critical importance to strengthen or rehabilitate the substandard RC beam-column joints. In this paper, a novel and practical method was experimentally investigated to rehabilitate damaged substandard interior reinforced concrete beam-column joints featured with no transverse reinforcement. The method applied engineered cementitious composite (ECC) to fill a steel cylinder shell to encase the joint zone. Test program consisted of three original and two rehabilitated, half-scale and three-dimensional, interior beam-column joint subassemblies subjected to cyclic loading with increasing amplitudes applied at beam ends. Three original specimens were constructed with no transverse reinforcement in their joint zones, in which one specimen had no slab and the other two were identical and constructed with slabs. The original specimens were first tested to failure and two of them were then rehabilitated using two ECC-infilled steel cylinder shells of different sizes for retesting. Forces, rebar strains, and displacements at loading points of beam ends were recorded during testing. Results found that the failure mode shifted from shear failure of joints in the original specimens to flexural failure of connected beam ends in the rehabilitated specimens. Peak values of interstory shear and corresponding deformability averaged an increase of about 41% and 39%, respectively. Stiffness improved about 33% at a drift ratio of about 0.035, compared to stiffness values of original specimens. The fully cumulative energy dissipation of the rehabilitated specimens was greater than that of the original specimens. The extra increase in interstory shear of 19% and the drift ratio of 21% were achieved by specimens with a large-scale cylinder shell compared to those of specimen with a small-scale cylinder shell, the large-scale cylinder shell can get a slightly better rehabilitation effect. In general, significant improvement in seismic resistance was achieved using the proposed rehabilitation method for substandard interior beam-column joints.

Keywords: Beam-column joint; Seismic retrofit; Engineered cementitious composite; Cylinder shell

1. Introduction

Reinforced concrete (RC) framed structures that were constructed prior to the 1970s usually do not meet current seismic design requirements. In particular, these structures constructed in earthquake-prone areas, e.g., the United States, New Zealand, Southeast Asia, and China, have significant deficiencies in the beam-column joint regions due to insufficient or no transverse reinforcement [1–6]. As a result, the substandard beam-column joints in existing structures are likely to fail in a brittle manner prior to the formation of plastic hinges in the connected beams. In some cases, the premature failure of these joints can lead to the entire collapse of buildings [7, 8]. Therefore, it is of critical importance to strengthen undamaged beam-column joints in earthquake-prone areas and to rehabilitate the damaged ones after an earthquake.

Efforts have been made to strengthen or rehabilitate the substandard RC beam-column joints in the last two decades. The purpose of these studies was to improve the load bearing capacity of joints and to avoid premature brittle failure (e.g., shear failure in joint zone). By doing this, a strength hierarchy could be established among the joint-connected columns and beams so that seismic strength and ductility demands could be accommodated in the form of a ductile beam hinging mechanism. Currently, several techniques for strengthening or rehabilitating the joints are available including concrete jacketing [9-11], steel jacketing and external steel elements [2,12-14], fiber reinforced polymer (FRP) composites [2, 5, 6, 15–17], diagonal metallic haunches [18–21], and planar joint expansion [22].

In the current study, a novel and practical seismic rehabilitation method for damaged substandard interior RC beam-column joints is proposed using an ECC-infilled steel cylinder shell. The purpose of this study is to reverse strength hierarchy by forming plastic hinges in beams while avoiding a premature failure in joint zones. The first step was to test original substandard beam-column joint specimens until failure under cyclic loading. The damaged specimens were then repaired and rehabilitated using the proposed method. The rehabilitated specimens were retested under the same loading protocol as that used for the original specimens. Finally, the rehabilitation effect was evaluated in terms of shear resistance, stiffness, and energy dissipation capacity.

2. Experimental program

The experimental program included three original and two rehabilitated interior beam-column joint subassemblies. These specimens were half-scale and three-dimensional including transverse beams. The fabricated longitudinal beams extended from joint edges to mid-length of the beams of the prototype structure, where the point of contraflexure was assumed to be located. Similar treatment was also applicable for the columns.

2.1 Original specimens

Fig. 1 illustrates the details of the geometry and reinforcement of the original specimens. Two identical beam-column joint subassemblies with 60-mm thick slabs were labeled as specimens JS1 and JS2. The third beam-column joint subassembly was designated as specimen J1. J1 had an identical joint zone, which connected beams and columns in the same manner as JS1 and JS2; however, J1 did not have a slab. By doing this, the contribution of the slab to the seismic behavior of the specimens could be investigated by comparing the test results of specimens JS1, JS2 and J1. The lengths of upper column, bottom column, longitudinal beams and transverse beams were 1000, 1400, 1525 and 675 mm, respectively. The cross-sectional dimensions of the columns and longitudinal beams were 250 × 250 mm and 150 × 280 mm, respectively. Each specimen had transverse beams with a cross-section of 100 × 150 mm. The longitudinal beams were reinforced with top rebars of 4D12 (four rebars with a diameter of 12 mm) and bottom bars of 3D12. The columns had a reinforcement of 12D12. The longitudinal reinforcement at the slab top was constructed using D6@200 (rebars with a diameter of 6 mm and an interval of 200 mm). Sufficient stirrups were provided in the columns and beams so that a premature shear failure prior to flexural failure was prevented. No transverse reinforcement was contained in the joint zones of the original specimens, which was intentionally omitted to achieve substandard beam-column joints. Table 1 presents the material properties of concrete and

reinforcing steel bars. Based on this information, the column-to-beam flexural strength ratios were calculated to be 1.45 and 2.10 for specimens JS1/JS2 and J1, respectively. In addition, the beam-column joint zones of the original specimens were calculated to be the weakest point of the beam-column joint subassemblies. Thus, all original specimens were expected to fail in joint shear mode.

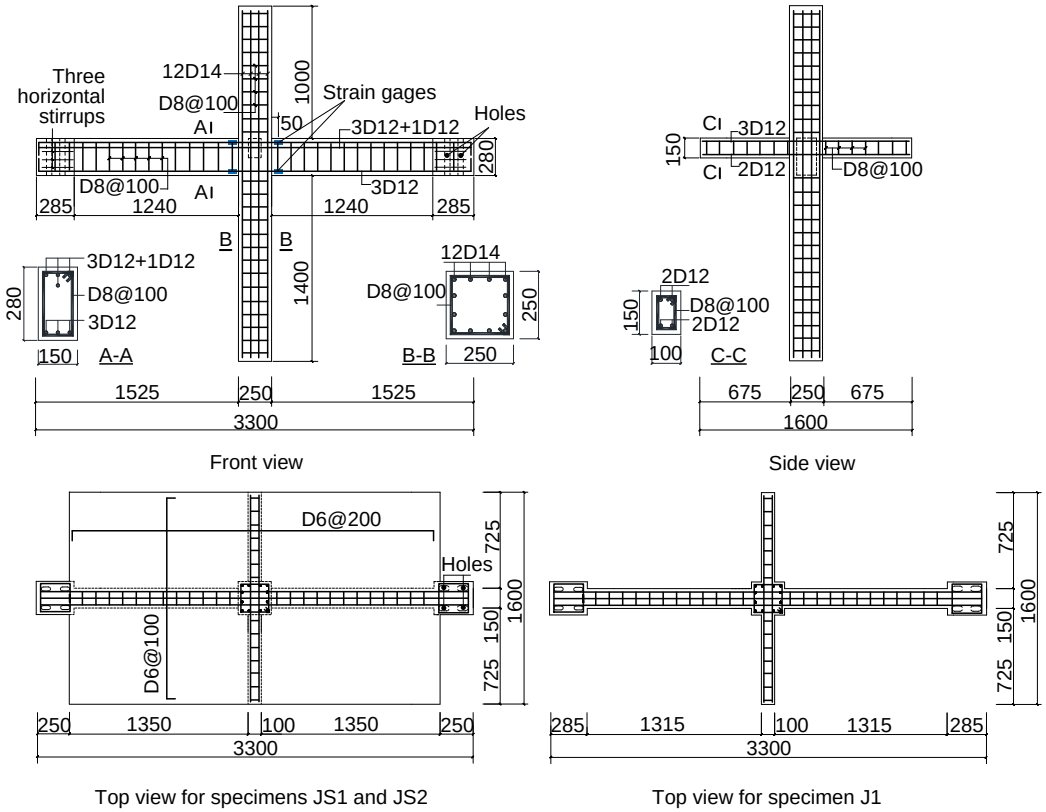

Fig. 1 – Geometries and reinforcements of the original specimens JS1, JS2 and J1

Table 1 – Material properties of concrete and reinforcing steel bars

Material	Parameter	Value			
Concrete	Uniaxial compressive strength (MPa)	21.1			
	Elasticity modulus ($\times 10^4$ MPa)	2.7			
Reinforcing steel bar		D14	D12	D8	D6
	Yield strength (MPa)	521	528	385	427
	Ultimate strength (MPa)	659	664	508	560
	Elasticity modulus ($\times 10^5$ MPa)	2.15	2.35	2.07	1.80
Steel in cylinder shell	Yield strength (MPa)	345			
	Ultimate strength (MPa)	470			
	Elasticity modulus ($\times 10^5$ MPa)	2.0			
ECC	Uniaxial compressive strength (MPa)	47.8			
	Elasticity modulus ($\times 10^4$ MPa)	2.2			
	Ultimate deflection (mm)	9.37			
	Ultimate tensile strain (%)*	1.1			
	Ultimate loads (N)	441			

*The value of the ultimate tensile strain was calculated using the inverse method proposed in [23], i.e., $\varepsilon=6.4 \cdot h \cdot f / l_0^2$, where h, f and l_0 are the height, ultimate deflection and support-to-support span of the specimen, respectively. A similar value was also obtained using the inverse method proposed in [24], as found by Pan et al. [25].

2.2 Rehabilitated specimens

The original specimens JS1 and JS2 were tested to failure and the damaged specimens were used to reconstruct rehabilitated specimens JS1-R and JS2-R, respectively. Fig. 2 illustrates the configuration of the steel cylinder shells which were applied to encase the beam-column joint zones and infilled with ECC. Each steel cylinder shell contained an enlarged body and two fixtures. Two inlet ports and four outlet ports were opened in the enlarged body for infilling ECC. Each enlarged body was assembled with two identical half parts which were clamped using eight 6-mm diameter bolts. The height of enlarged bodies was 320 mm and their diameters were 450 mm and 500 mm for specimens JS1-R and JS2-R, respectively. The steel shell and base plate of the enlarged bodies were 8 mm thick and the other parts were 5 mm thick. Ribs were set on the internal surface of each cylinder shell to enhance the bond behavior between the enlarged body and ECC. Two U-shaped steel fixtures were used to further clamp the enlarged body with longitudinal beam ends so that the two parts of the enlarged body did not separate from each other during loading. The material properties of steel to construct the cylinder shell are presented in Table 1.

Eco-friendly and cost-effective polyvinyl alcohol (PVA) fibers with excellent alkali resistance were used to produce ECC (PVA-ECC). Table 2 presents the mix proportion of the PVA-ECC. Critical parameters of properties were averaged and are presented in Table 1.

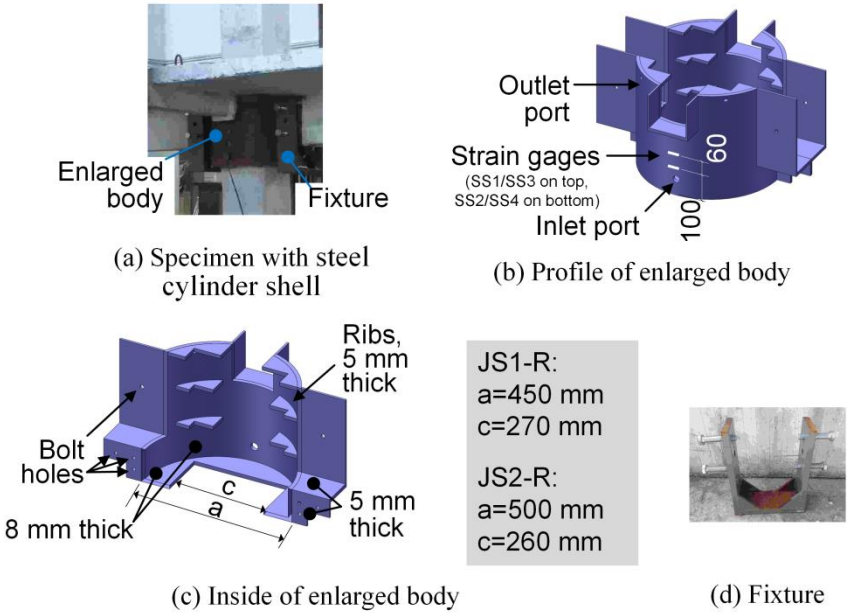

(a) Specimen with steel cylinder shell

(b) Profile of enlarged body

(c) Inside of enlarged body

(d) Fixture

Fig. 2 – Configuration of steel cylinder shells for specimens JS1-R and JS2-R

Table 2 – Mix proportion of PVA-ECC (weight ratios)

Cement (Portland, P.II.42.5)	Fly ash	Sand-binder* ratio	Water-binder* ratio	Water reducing admixture	V_f #(%)
1.0	2.4	0.36	0.28	0.013-0.018	2.0

*Binder comprises cement and fly ash. #V_f is fiber volume fraction.

A construction approach was performed to repair and retrofit the damaged specimens JS1 and JS2 to build the rehabilitated specimens JS1-R and JS2-R. This approach contained several steps including specimen repair, cylinder shell installation, ECC grouting, and curing. The procedures are as follows: 1) Loose concrete was removed from the joint zones of damaged specimens JS1 and JS2 after testing and the joint surfaces were cleared using water. Cracks were then infilled with epoxy resin by pressure injection. Afterward fine aggregate concrete was used to repair the joint zones to recover their original dimension. The compressive strength of the fine aggregate concrete was slightly higher than that of the concrete used in the

original specimens. 2) The prefabricated steel cylinder shells were installed to encase the damaged beam-column joint zones. For each specimen, eight through bolts and two fixtures were used to assemble the enlarged bodies of the cylinder shells. The gaps between steel plates and beam surfaces were infilled using epoxy adhesive. Rubber bands were temporarily used to fill up the gaps between the bottom plate of the enlarged bodies and the column surfaces. 3) After properly curing the fine aggregate concrete and epoxy resin, ECC was grouted from the inlet ports. 4) The rehabilitated specimens were cured in a natural environment for 28 days until testing.

2.3 Test setup, loading history and instrumentation

Fig. 3 illustrates the test setup for the original and rehabilitated specimens. The head and foot of the column were supported by a roller and hinge, respectively. The column head was against horizontal displacement and the column foot was restrained in both vertical and horizontal directions. A constant axial load of 300 kN was imposed on the column head using a hydraulic jack to simulate gravity action. This axial load represents about 23% of the axial compressive capacity of the column. Each beam end was pin-connected to a hydraulic actuator with a ± 100 kN loading capacity and a ± 200 mm displacement range. Quasi-static cyclic loads were applied on the beam ends in two opposite directions, i.e., alternatively pulling down on one beam end and pushing up the other. Positive and negative loading directions denoted downward and upward motions, respectively, as demonstrated in Fig. 3.

Fig. 4 presents the loading history in accordance with the Chinese code [26]. Force control mode was used for Cycles 1, 2, and 3 with a force magnitude of $0.5P_y$, $0.75P_y$ and P_y, respectively, where yielding force P_y meant the estimated force when the tested specimen yielded. Afterwards, the displacement control mode was used for loading with incremental displacement magnitudes of Δ_y, $2\Delta_y$, $3\Delta_y$…, where Δ_y denoted the displacement when the specimen yielded. The loop was repeated three times at each displacement magnitude in the loading phase of the displacement control mode. For each specimen, the loading was stopped when the specimen lost 15% of its peak resistance.

Forces, rebar strains, and displacements at loading points of beam ends were recorded during testing. The constant axial load imposed on the column top was monitored and the loads applied at the beam ends were measured. For each specimen, two displacement meters, *D*1 and *D*2, were used to measure the displacements at the loading points of beam ends, as illustrated in Fig. 3. A data acquisition system was used to record the forces, rebar strains, and displacements.

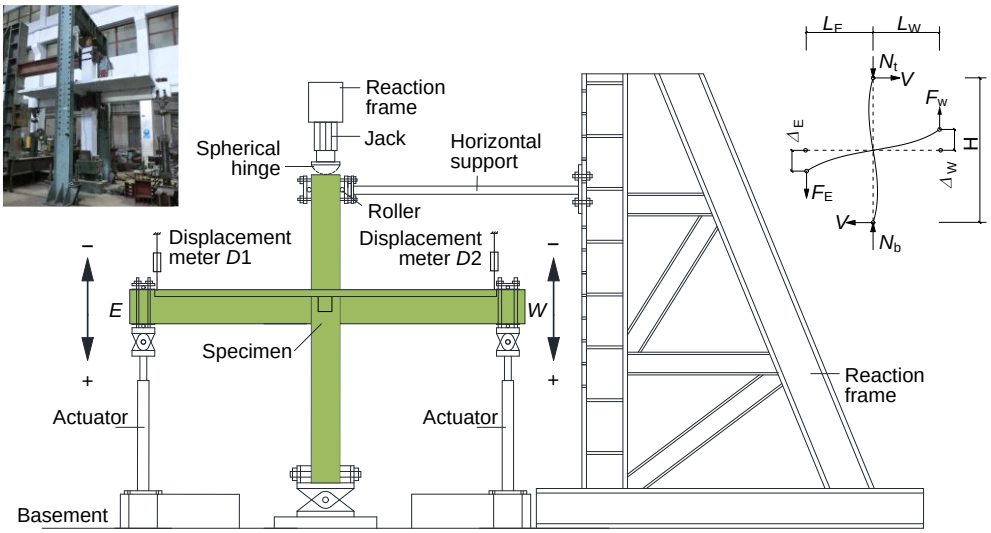

Fig. 3 – Test setup for original and rehabilitated specimens

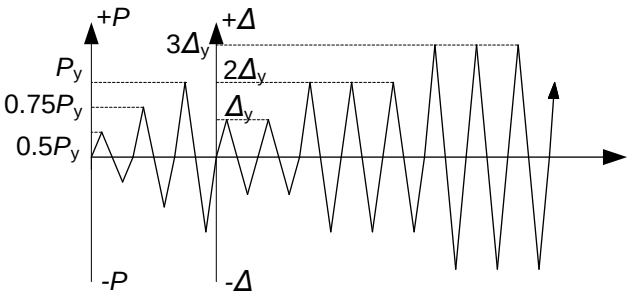

Fig. 4 – Loading history

3. Test results and observations

The general behavior of all specimens is described in terms of cracking development, force-displacement hysteretic responses, and reinforcement strains. The force-displacement hysteretic responses were depicted using the forces and displacements measured at the beam ends.

3.1 Original specimens JS1, JS2 and J1

Fig.5 presents the failure profile after testing. For identical specimens JS1 and JS2, a similar cracking development occurred. Both specimens behaved elastically and no cracking was observed after the first loading cycle (i.e., Cycle 1) with force magnitudes of +15 and −10 kN. Fine cracks initiated in the joint zones and slabs after the second cycle with force magnitudes of +22.5 and −15 kN. As loads increased, more cracks commenced and developed in joint zones to gradually form an X-shaped pattern, which is a typical failure profile in joint zones. The concrete in the joint zones spalled and crushed off and longitudinal reinforcements in the columns were visible. Number, length and width of cracks in the slabs, beams and columns also developed continuously with the increasing of loads. For specimen J1, no cracking was observed after the first loading cycle with force magnitudes of +10 and −7.5 kN. Slight diagonal cracks appeared in the joint zone after the second cycle with force magnitudes of +15 and −11.25kN. As loads increased, these diagonal cracks grew in size and number and finally formed a typical X-shaped pattern. Cracks were also observed in the beams and columns; however, they became stable and did not cause the failure of the beams and columns. Evidently, the joint shear failure was identified as the failure mode for specimens JS1, JS2, and J1.

Fig. 5 – Failure profiles of specimens after testing

Fig. 6 illustrates the force-displacement hysteretic responses. The positive peak loads of about 41, 44, and 27 kN were reached at displacements of about 47, 45, and 39 mm, respectively. Meanwhile the negative peak loads of −35, −38, and −29 kN were achieved at displacements of −43, −39, and −48 mm for specimens JS1, JS2 and J1, respectively. Compared to specimen J1 without slab, the positive and negative peak loads of specimens constructed with slabs had an average increase of about 57% and 26%, respectively. This confirmed the considerable contribution of slabs to the resistance of beam-column joints [27]. In addition, continuous degradation of both resistance and stiffness after peak loads were also observed. Furthermore, all curves exhibited a pinching effect, due mainly to a degeneration of the bond-slip behavior of the longitudinal reinforcements and the increase of concrete cracking in joint zones and beam ends [14].

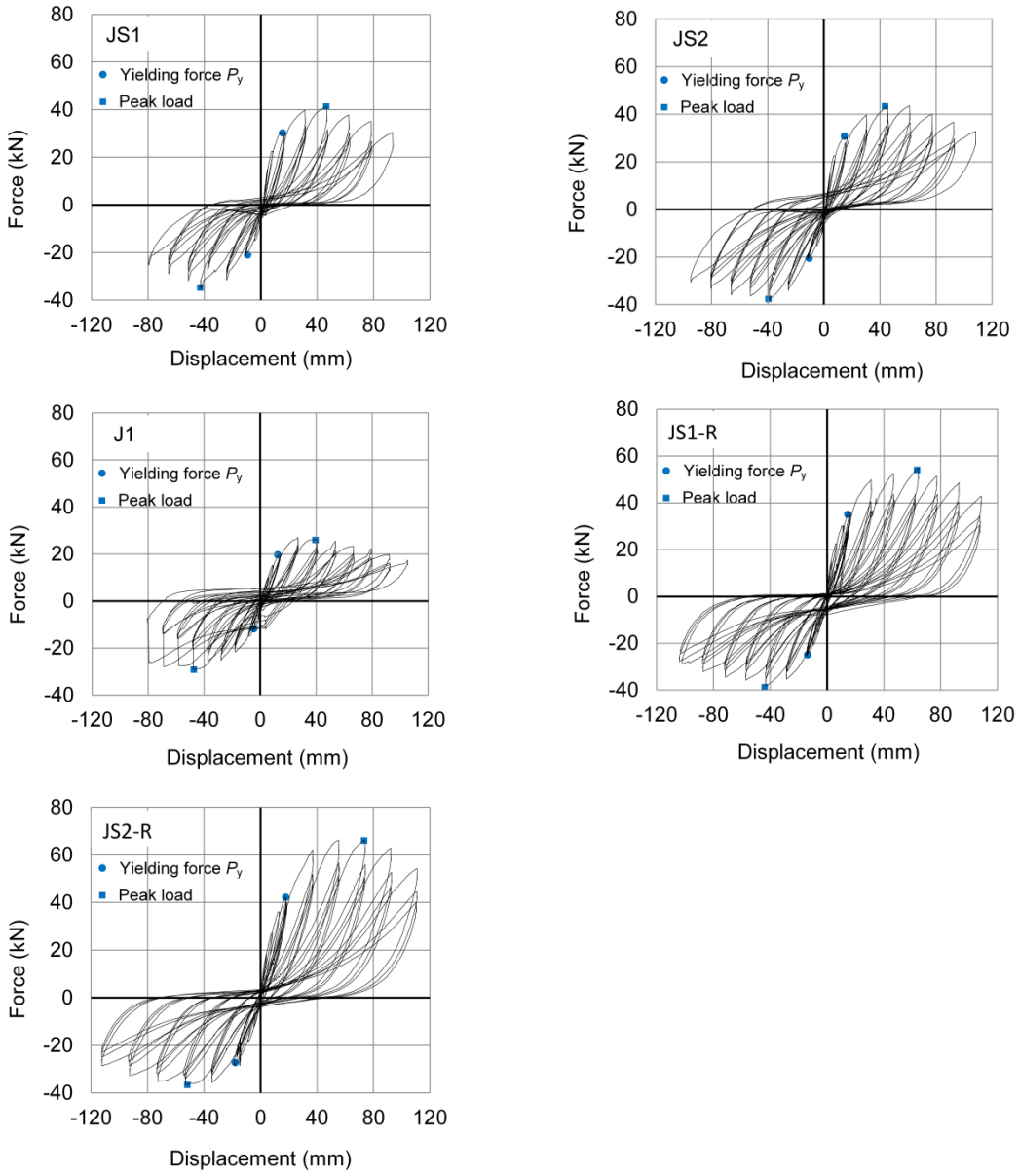

Fig. 6 – Load-displacement hysteretic responses

3.2 Rehabilitated specimens JS1-R and JS2-R

Fig. 5 presents the failure profile after testing for specimens JS1-R and JS2-R which showed similar behavior during the cracking development. Cracks initiated in the bottom and lateral surfaces of the beam as well as at

the column ends adjacent to the joint zone after the second loading cycle. As loads increased, cracks grew in size and number in the beam and column regions close to the joint zone. Concrete spalled and crushed off in these regions when peak loads were reached. After that, the two half parts of the enlarged bodies tended to separate from each other because the gap between them was wide. However, no separation was observed.

Fig. 6 illustrates the force-displacement hysteretic responses for specimens JS1-R and JS2-R. The positive peak loads of 55 and 66 kN were reached at displacements of 64 and 74 mm, respectively. At the same time, the negative peak loads of −38 and −37 kN commenced at displacements of −43 and −52 mm for specimens JS1-R and JS2-R, respectively. Compared to the mean values of the original specimens, the positive peak load of specimen JS1-R increased approximately 29%. The responding value was 55% for specimen JS2-R. This indicated, in a preliminary sense, the significant effectiveness of the rehabilitation method because the shear resistance of damaged joints not only recovered but was also enhanced. However, the pinching effect of the rehabilitated specimens did not seem to improve compared to that of the original specimens. This is because the degradation of bond-slip behavior of longitudinal reinforcement in joint zones and beam ends, as well as concrete cracking in beam ends, could hardly be improved using the proposed method.

4. Discussion on rehabilitation effect

Fig. 7 illustrates the interstory shear–drift ratio envelope curves of the five specimens which are the essential responses of beam-column joints under lateral forces. It was found that: 1) The profiles of each curve under positive and negative loadings were similar and, thus, their curves under positive loading were used for analysis of interstory shear in this subsection for brevity. For specimens JS1, JS2, JS1-R and JS2-R, the peak values of the interstory shears were about 41, 45, 56, and 64 kN with their corresponding drift ratios of 0.035, 0.040, 0.048, and 0.056, respectively. 2) The nominal shear stress of joint zones [28, 29] of specimens JS1, JS2 and J1 were $0.33f_c$, $0.36f_c$ and $0.24f_c$ (f_c denotes the uniaxial compressive strength of concrete) which were comparable to the previous results, e.g., in [4, 30], with consideration of the presence of transverse beams and slabs. 3) Compared to the average value of the original specimens, the peak values of the interstory shear of the rehabilitated specimens JS1-R and JS2-R increased 31% and 50% with a mean value of 41%, and their drift ratios improved 28% and 49% with an average value of 39%, respectively. These results revealed that the extra increase in interstory shear of 19% and the drift ratio of 21% were achieved by specimens JS2-R equipped with a large-scale cylinder shell compared to those of specimen JS1-R with a small-scale cylinder shell. 4) For specimen J1, the peak value of the interstory shear was 30.0 kN with a drift ratio of 0.026. Both values were significantly less than those of specimens JS1 and JS2, indicating a considerable contribution of the slab to the shear resistance and deformability of beam-column joints.

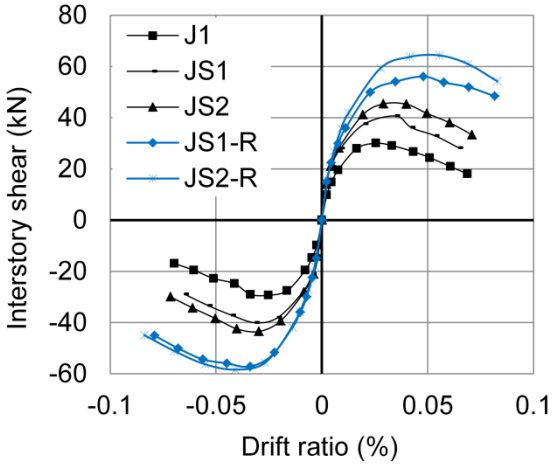

Fig.7 – Interstory shear–drift ratio envelope curves for specimens JS1, JS2, J1, JS1-R and JS2-R

The stiffness of a beam-column joint under the *i*th loading cycle, K_i, was approximated as the slope of the peak-to-peak line in each loading cycle and calculated using Eq. (1) [26]:

$$K_i = \frac{|F_i^+| + |F_i^-|}{|d_i^+| + |d_i^-|} \quad (1)$$

where F_i^+ and d_i^+ denote the peak values of the interstory shear and drift ratio in the positive direction in the *i*th loading cycle, respectively; and F_i^- and d_i^- refer to the corresponding values in the negative direction, respectively. Fig. 8 illustrates the stiffness degradation for specimens JS1, JS2, J1, JS1-R and JS2-R where only the first cycle of each loading magnitude was considered. Results revealed that: 1) Stiffnesses of the rehabilitated specimens JS1-R and JS2-R were generally larger than those of the original specimens JS1 and JS2. As an example, the stiffness of specimens JS1-R and JS2-R increased by an average of 33% compared to the average stiffness of specimens JS1 and JS2 at a drift ratio of about 0.035. 2) Specimen JS2-R had a slightly larger stiffness compared to that of specimen JS1-R which attributed to the size difference in their enlarged bodies. 3) The respective stiffness of specimens JS1 and JS2 were larger than the stiffness of specimen J1 due to their slabs resistance to shear.

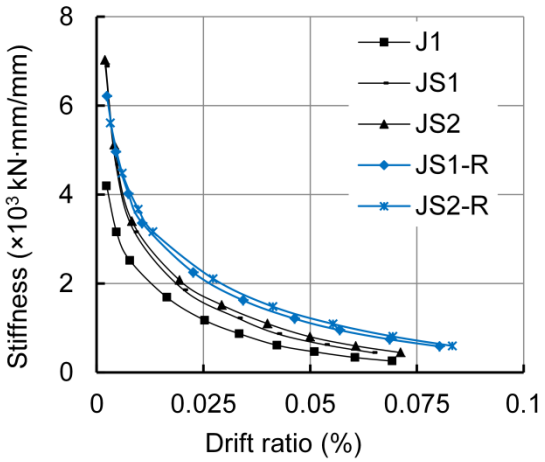

Fig.8 – Stiffness degradation curves for specimens JS1, JS2, J1, JS1-R and JS2-R

The dissipated energy in the *i*th loading cycle, E_i, is represented by the area enclosed by the complete hysteretic loop of the *i*th loading cycle in the interstory shear–drift ratio curves, as illustrated in Fig. 9 [31]. Thus, the cumulative energy dissipation is calculated through summation of the dissipated energy in each experienced loading cycle. Fig. 9 presents the cumulative energy dissipation for specimens JS1, JS2, J1, JS1-R and JS2-R. It was found that: 1) Energy dissipation capacity in the first few loading cycles of rehabilitated specimens was comparable to that of original specimens. However, the fully cumulative energy dissipation of the rehabilitated specimens was greater than that of the original specimens due to improved deformability of the rehabilitated specimens. 2) No appreciable distinction was observed between specimens JS1-R and JS2-R. These two observations were due partially to the generally elastic behavior of the ECC-infilled steel cylinder shell and serious pinching effect of the rehabilitated specimens. 2) The presence of slabs in beam-column joints contributed significantly to energy dissipation based on the comparison between the test results of specimens JS1/JS2 and J1.

In summary, the specimens rehabilitated by ECC-infilled steel cylinder shells exhibited excellent performance in terms of shear resistance, stiffness and energy dissipation capacity. The main reasons were that: 1) The joint zones were enlarged with steel cylinder shell and high-performance material of ECC, leading to a decrease in shear stress in the joint zones, an increase in stiffness and, therefore, improvement of cumulative energy dissipation. 2) The performance of the core joint zones of the original specimens was enhanced because they were intensively restrained by the infilled ECC in three dimensions. Besides, a comparison on the rehabilitation effect using the proposed method with that in the literature was currently

unavailable due to different specimens that were used, e.g., interior and exterior joints, with and without slabs, damaged and intact joints. Finally, reinforcement ratios of the connected components (1.1% for beam ends and 2.9% for columns) and the column-to-beam flexural strength ratios of the original specimens (2.10 for specimens JS1/JS2 and 1.45 for specimen J1) were typical for practical structures, which indicated a wide application of the proposed method.

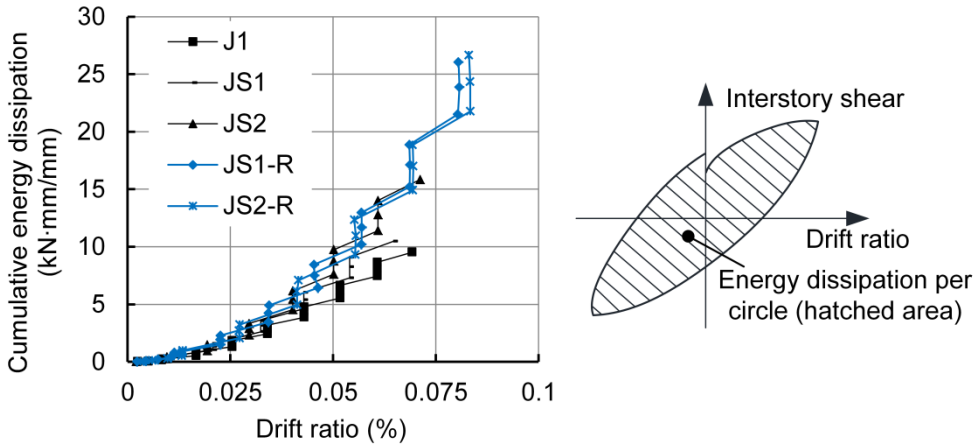

Fig. 9 – Energy dissipation for specimens JS1, JS2, J1, JS1-R and JS2-R

5. Conclusions

Based on the test results, the following conclusions are drawn:

(1) The failure mode was changed from joint shear failure in the original specimens to flexural failure in beams in the rehabilitated specimens featured with plastic hinges forming in beam ends. This meant the hierarchy of strength related to the connected components was properly established and a premature failure of the joint zone was prevented after rehabilitation.

(2) The rehabilitated specimens displayed an enhanced performance compared to the original ones. For rehabilitated specimens, their peak values of interstory shear and corresponding deformability increased by an average of about 41% and 39%, respectively, and stiffness improved by about 33% at a drift ratio of about 0.035, compared to those of the original specimens. Cumulative energy dissipation capacity of the rehabilitated specimens was significantly greater than that of the original specimens.

(3) A slightly better rehabilitation effect was confirmed for a specimen equipped with a large-scale enlarged body.

(4) The presence of slabs significantly contributed to the performance of the beam-column joints.

References

[1] Park R (2002): A summary of results of simulated seismic load tests on reinforced concrete beam-column joints, beams and columns with substandard reinforcing details. *Journal of Earthquake Engineering*, 6(2), 1–27.

[2] Engindeniz M, Kahn LF, Abdul-Hamid Z (2005): Repair and strengthening of reinforced concrete beam-column joints: State of the art. *ACI Structural Journal*, 102(2), 187–197.

[3] Supaviriyakit T, Pimanmas A (2008): Comparative performance of sub-standard interior reinforced concrete beam-column connection with various joint reinforcing details. *Materials and Structures*, 41(3), 543–557.

[4] Li, B, Ngoc CT, Pan TC (2009): Experimental and numerical investigations on the seismic behavior of lightly reinforced concrete beam-column joints. *Journal of Structural Engineering*, 135(9), 1007–1018.

[5] Hadi MNS, Tran TM (2016): Seismic rehabilitation of reinforced concrete beam-column joints by bonding with concrete covers and wrapping with FRP composites. *Materials and Structures*, 49(1-2), 467–485.

[6] Lu ZD, Xie LP, Hong T (2003): A seismic research on beam-column-slab subassemblies reinforced with low ratio transverse reinforcement rehabilitated by carbon fiber reinforced plastic. *Journal of Tongji University*, 31(3), 253–257 [in Chinese].

[7] Ghobarah A, Said A (2002): Shear strengthening of beam-column joints. *Engineering Structures*, 24(7), 881–888.

[8] Yap SL, Li B (2011): Experimental investigation of reinforced concrete exterior beam-column subassemblages for progressive collapse. *ACI Structural Journal*, 108(5), 542–552.

[9] Alcocer SM, Jirsa JO (1993): Strength of reinforced-concrete frame connections rehabilitated by jacketing. *ACI Structural Journal*, 90, 249–61.

[10] Karayannis CG, Chalioris CE, Sirkelis GM (2008): Local retrofit of exterior RC beam-column joints using thin RC jackets – an experimental study. *Earthquake Engineering & Structural Dynamics*, 37, 727–46.

[11] Tsonos ADG (2010): Performance enhancement of R/C building columns and beam-column joints through shotcrete jacketing. *Engineering Structures*, 32, 726–40.

[12] Bracci JM, Reinhorn AM, Mander JB (1995): Seismic retrofit of reinforced concrete buildings designed for gravity loads: performance of structural model. *ACI Structural Journal*, 92, 711–23.

[13] Ghobarah A, Aziz TS, Biddah A (1997): Rehabilitation of reinforced concrete frame connections using corrugated steel jacketing. *ACI Structural Journal*, 94, 283–94.

[14] Shafaei J, Hosseini A, Marefat MS (2014): Seismic retrofit of external RC beam-column joints by joint enlargement using prestressed steel angles. *Engineering Structures*, 81, 265–288.

[15] El-Amoury T, Ghobarah A (2002): Seismic rehabilitation of beam-column joint using GFRP sheets. *Engineering Structures*, 24, 1397–407.

[16] Pantelides CP, Okahashi Y, Reaveley LD (2008): Seismic rehabilitation of reinforced concrete frame interior beam-column joints with FRP composites. *Journal of Composites for Construction*, 12, 435–445.

[17] Beydokhti EZ, Shariatmadar H (2016): Strengthening and rehabilitation of exterior RC beam-column joints using carbon-FRP jacketing. *Materials and Structures*, 49(12), 5067–5083.

[18] Pampanin S, Christopoulos C, Chen TH (2006): Development and validation of a metallic haunch seismic retrofit solution for existing under-designed RC frame buildings. *Earthquake Engineering & Structural Dynamics*, 35, 1739–66.

[19] Said A, Nehdi M (2008): Rehabilitation of RC frame joints using local steel bracing. *Structure and Infrastructure Engineering*, 4, 431–47.

[20] Sharbatdar MK, Kheyroddin A, Emami E (2012): Cyclic performance of retrofitted reinforced concrete beam-column joints using steel prop. *Construction and Building Materials*, 36, 287–94.

[21] Wang B, Zhu S, Xu YL, Jiang HJ (2018): Seismic retrofitting of non-seismically designed RC beam-column joints using buckling restrained haunches: design and analysis. *Journal of Earthquake Engineering*, 22(7), 1188–1208.

[22] Chaimahawan P, Pimanmas A (2009): Seismic retrofit of substandard beam-column joint by planar joint expansion. *Materials and Structures*, 42(4), 443–459.

[23] Cai XR, Xu SL (2010): Study on corresponding relationships between flexural load deformation hardening curves and tensile stress-strain hardening curves of UHTCC. *Engineering Mechanics*. 27(1), 8–16 [in Chinese].

[24] Qian SZ, Li VC (2007): Simplified inverse method for determining the tensile strain capacity of strain hardening cementitious composites. *Journal of Advanced Concrete Technology*, 5(2), 235–246.

[25] Pan ZF, Wu C, Liu JZ, Wang W, Liu JW (2015): Study on mechanical properties of cost-effective polyvinyl alcohol engineered cementitious composites (PVA-ECC). *Construction and Building Materials*, 78, 397–404.

[26] Ministry of Housing and Urban-Rural Development of the People's Republic of China (2015): Specification for seismic test of buildings (JGJ/T 101-2015), Beijing, China [in Chinese].

[27] Pantazopoulou SJ, French CW (2001): Slab participation in practical earthquake design of reinforced concrete frames. *ACI Structural Journal*, 98(4), 479–489.

[28] American Concrete Institute (2011): Building code requirements for structural concrete and commentary (ACI 318-11), American Concrete Institute, Farmington Hills, MI..

[29] Ministry of Construction of China and State Bureau of Quality and Technical Supervision of China (2002): Code for design of concrete structures (GB50010-2002), Beijing, China [in Chinese].

[30] Hakuto S, Park R, Tanaka H (2000): Seismic load tests on interior and exterior beam-column joints with substandard reinforcing details. *ACI Structural Journal*, 97, 11-25.

[31] Priestley MJN, Seible F, Calvi GM (1996): Seismic design and retrofit of bridges, John Wiley & Sons, New York.